Open access • Journal Article • DOI:10.1615/INTERJFLUIDMECHRES.V32.I3.10

Transient Free Convection Flow of a Micropolar Fluid Over a Vertical Surface

Hamzeh Mustafa Duwairi, Ali J. Chamkha

Institutions: University of Jordan, American University of Ras Al Khaimah

Published on: 01 Jan 2005 - International Journal of Fluid Mechanics Research (Begel House Inc.)

Topics: Combined forced and natural convection, Natural convection, Rayleigh number, Boundary layer and Rayleigh–Bénard convection

Available online at http://ijim.srbiau.ac.ir

Int. J. Industrial Mathematics Vol. 1, No. 4 (2009) 291-305

Free Convective Flow of a Micropolar Fluid along an Elliptic Cylinder in Porous Media Using the Thermal Non-Equilibrium Model

Ali J. Chamkha [a]*; R.A. Mohamed [b], S.E. Ahmed [b]

(a) *Manufacturing Engineering Department, The Public Authority for Applied Education and Training Shuweikh 70654, Kuwait*

(b) *Department of Mathematics, South Valley University, Qena, Egypt.*

Received 20 September 2009; accepted 29 Desember 2009.

Abstract

This work uses the thermal non-equilibrium model to study free convection boundary-layer flow of a micropolar fluid along a cylinder of elliptic cross-section embedded in porous media. The transformed conservation equations of the non-similar boundary layers are solved numerically by an efficient, iterative, tri-diagonal implicit finite difference method. The numerical results are compared and found to be in excellent agreement with previously published results on special cases of the problem. The obtained results are displayed graphically to illustrate the influence of the different physical parameters on the linear and angular velocities and the fluid- and solid-phase temperatures, as well as the local skin-friction coefficient, wall couple stress coefficient and the local Nusselt numbers for fluid and solid phases.

Keywords : Free convection; Elliptic cylinder; Micropolar fluid; Porous media; Thermal non-equilibrium model.

1 Introduction

The classical Navier-Stokes theory does not describe adequately the flow properties of polymeric fluids, colloidal suspensions, and fluids containing certain additives. Eringen [1] proposed the theory of micropolar fluids which includes micro-rotation as well as micro-inertia effects. The theory of thermo-micropolar fluids was also developed by Eringen [2] by extending his theory of micropolar fluids. The theory of micropolar fluids is generating

*Corresponding author. Email address: achamkha@yahoo.com

a lot of interest and many classical flows are being re-examined to determine the effects of micro-structure.

On the other hand, in modeling flows in porous media, the utilization of the assumption of local thermal equilibrium between the fluid and the solid porous medium breaks down often in many practical applications. Quintard and Whitaker [3] cited numerous physical situations where local thermal equilibrium fails. For example, when there is a significant heat generation occurring in any one of the two phases (solid or fluid), the temperatures in the two phases are no longer identical. When the temperature at the bounding surface changes significantly with respect to time, and when solid and fluid phases have significantly different heat capacities and thermal conductivities, the local rate of change of temperature for one phase differs significantly from that for the other phase. Amiri and Vafai [4] investigated the validity of local thermal equilibrium conditions for steady state as well as transient incompressible flow through a porous medium. Kim et al. [5] presented an analytical solution for the two-equation model including the boundary effect for an equivalent micro-channel application. They presented analytical solutions for the fluid- and solid-phase temperature distributions based on the Brinkman-extended Darcy equation. They also analyzed the validity of the local thermal equilibrium assumption.

In the absence of local thermal equilibrium, the single energy equation needs to be replaced with two energy equations, one for the solid and another for the fluid. The coupling of these two equations is given by the interfacial heat transfer coefficient. Two energy equation models have been introduced heuristically in the literature [6]. In recent years, the local thermal non-equilibrium model has been given considerable attention and has been utilized in various fields [7] due to its pertinence in applications. For example, Lee and Vafai [8] employed the thermal non-equilibrium model to investigate the forced convection flow through a channel filled with a porous medium. They obtained analytical solutions for the fluid- and solid-phase temperature distributions.

The objective of this paper is to study the thermal non-equilibrium model for heat transfer by free convection from cylinders of elliptic cross-section in micropolar fluid through a porous medium. An appropriate coordinate transformation and an adequate implicit finite-difference method are applied to study this problem. The influence of vertex viscosity parameter, permeability parameter, heat transfer coefficient parameter, thermal conductivity ratio, and the aspect ratio on heat transfer characteristics, linear velocity and angular velocity are examined for both cases when the major axis is horizontal (blunt orientation) and when the major axis is vertical (slender orientation).

2 Governing equations

The configuration considered is a horizontal cylinder of elliptic cross-section which is situated in a micropolar fluid as shown in Fig. 1, where coordinates are measured along the surface of the cylinder and normal to it, respectively. is the angle made by the outward normal from the cylinder with the downward vertical and is the eccentric angle. We assume that the surface of the cylinder is maintained at a uniform temperature which is higher than the ambient fluid temperature

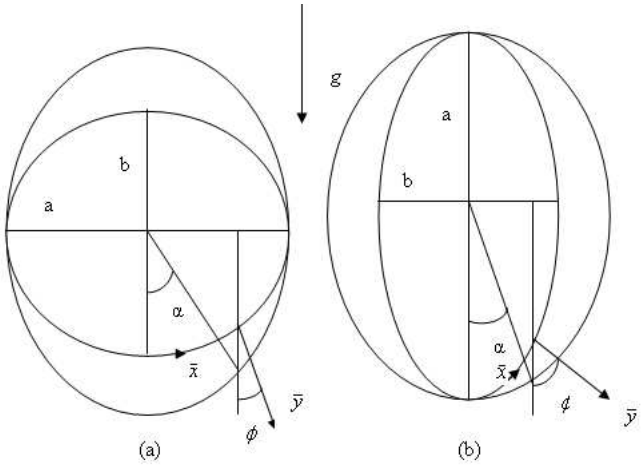

Fig. 1. Physical model and coordinate system: (a) blunt orientation; (b) slender orientation

Using the thermal non-equilibrium model and the Boussinesq approximation, we can write the governing equations in two-dimensional Cartesian coordinates as:

$$\frac{\partial \bar{u}}{\partial \bar{x}} + \frac{\partial \bar{v}}{\partial \bar{y}} = 0, \tag{2.1}$$

$$\bar{u}\frac{\partial \bar{u}}{\partial \bar{x}} + \bar{v}\frac{\partial \bar{u}}{\partial \bar{y}} = (\upsilon + \frac{k}{\rho})\frac{\partial^2 \bar{u}}{\partial \bar{y}^2} + g\beta[T_f - T_\infty]\sin\phi + \frac{k}{\rho}\frac{\partial \bar{N}}{\partial \bar{y}} - \frac{\upsilon}{k_1}\bar{u}, \tag{2.2}$$

$$\bar{u}\frac{\partial \bar{N}}{\partial \bar{x}} + \bar{v}\frac{\partial \bar{N}}{\partial \bar{y}} = \frac{\gamma}{\rho j}\frac{\partial^2 \bar{N}}{\partial \bar{y}^2} - \frac{k}{\rho j}(\frac{\partial \bar{u}}{\partial \bar{y}} + 2\bar{N}), \tag{2.3}$$

$$\bar{u}\frac{\partial T_f}{\partial \bar{x}} + \bar{v}\frac{\partial T_f}{\partial \bar{y}} = \frac{\varepsilon k_f}{(\rho c_p)_f}\frac{\partial^2 T_f}{\partial \bar{y}^2} + \frac{h}{(\rho c_p)_f}\left[T_s - T_f\right], \tag{2.4}$$

$$[1-\varepsilon]k_s\frac{\partial^2 T_s}{\partial \bar{y}^2} + h\left[T_f - T_s\right] = 0. \tag{2.5}$$

In the above equations, $(\bar{u}, \bar{v})$are the velocity components along the $(\bar{x}, \bar{y})$ axes, $\bar{N}$ is the angular velocity of the micropolar fluid, k is the vortex-viscosity, j is the micro-inertia, γ is the spin gradient viscosity, $T_f$and $T_s$are the fluid- and solid-phase temperatures, respectively, $k_f$and $k_s$are the fluid- and solid-phase thermal conductivities, respectively, h is the heat transfer coefficient between the solid and fluid phase, k_1 is the permeability of the porous medium, υ is the kinematic viscosity of the fluid, $g$is the gravitational acceleration, β is the coefficient of volume expansion, $\rho_f$and $c_{p_f}$are the density and constant-pressure specific heat of the fluid, respectively, and ε is the porosity of the porous medium.

The appropriate boundary conditions are

$$\begin{array}{ll} \bar{u} = \bar{v} = 0, \quad T_f = T_w, \quad T_s = T_w, \quad \bar{N} = -n\frac{\partial \bar{u}}{\partial \bar{y}} & on \quad \bar{y} = 0 \\ \bar{u} = 0, \quad T_f = T_\infty, \quad T_s = T_\infty, \quad \bar{N} = 0 & as \ \bar{y} \to \infty, \end{array} \tag{2.6}$$

where $0 \le n \le 1$. The case $n = 0$, which indicates $N = 0$, represents concentrated particle flow in which the microelements close to the wall surface are unable to rotate. The case $n = 1/2$ indicates the vanishing of the anti-symmetric part of the stress tensor and denotes weak concentrations. The case $n = 1$ is used for modeling turbulent boundary layer flows.

The above equations are further non-dimensionalized using the definitions

$$\begin{aligned} &x = \bar{x}/a, \quad y = (\bar{y}/a)Gr^{1/4}, \quad \psi = (\bar{\psi}/v)Gr^{-1/4} \\ &N = (a^2\bar{N}/v)Gr^{-3/4}, \quad \theta_f = (T_f - T_\infty)/(T_w - T_\infty), \\ &\theta_s = (T_s - T_\infty)/(T_w - T_\infty), \end{aligned} \tag{2.7}$$

where $Gr = g\beta(T_f - T_\infty)a^3/v^2$ is the Grashof number and $\bar{\psi}$is the stream function which is defined in the usual way $(\bar{u}, \bar{v}) = (\partial\bar{\psi}/\partial\bar{y}, -\partial\bar{\psi}/\partial\bar{x})$. Substitution of Equations(2.7) into Equations (2.2)-(2.5) leads to

$$\frac{\partial\psi}{\partial y}\frac{\partial^2\psi}{\partial y\partial x} - \frac{\partial\psi}{\partial x}\frac{\partial^2\psi}{\partial y^2} = (1+\Delta)\frac{\partial^3\psi}{\partial y^3} + \Delta\frac{\partial N}{\partial y} + \theta_f \sin\phi - K_1\frac{\partial\psi}{\partial y}, \tag{2.8}$$

$$\frac{\partial\psi}{\partial y}\frac{\partial N}{\partial x} - \frac{\partial\psi}{\partial x}\frac{\partial N}{\partial y} = \lambda\frac{\partial^2 N}{\partial y^2} - B.\Delta\left[2N + \frac{\partial^2\psi}{\partial y^2}\right], \tag{2.9}$$

$$\frac{\partial\psi}{\partial y}\frac{\partial\theta_f}{\partial x} - \frac{\partial\psi}{\partial x}\frac{\partial\theta_f}{\partial y} = \frac{1}{\mathrm{Pr}}\left[\frac{\partial^2\theta_f}{\partial y^2} + H[\theta_s - \theta_f]\right], \tag{2.10}$$

$$\frac{\partial^2\theta_s}{\partial y^2} - \chi H[\theta_s - \theta_f] = 0, \tag{2.11}$$

where $\mathrm{Pr} = (\mu c_p)_f/\varepsilon k_f$is the Prandtl number, $H = (ha^2/\varepsilon k_f)Gr^{-1/2}$ is the heat transfer coefficient parameter, $\chi = k_f/\varepsilon k_s(1-\varepsilon)$ is the thermal conductivity ratio parameter, $\Delta = k/\mu$is the vortex-viscosity parameter, $\lambda = \gamma/\mu j$ is the micro-rotation parameter, $B = (a^2/j)Gr^{-1/2}$ is the material parameter and $K_1 = (a^2/k_1)Gr^{-1/2}$ is the permeability parameter.

The dimensionless form of the boundary conditions (2.6) become

$$\begin{aligned} &\tfrac{\partial\psi}{\partial y} = \tfrac{\partial\psi}{\partial x} = 0, \quad \theta_f = 1, \quad \theta_s = 1, \quad N + n\tfrac{\partial^2\psi}{\partial y^2} = 0 \quad on \;\; y = 0, \\ &\tfrac{\partial\psi}{\partial y} = 0, \quad \theta_f = 0, \quad \theta_s = 0, \quad N = 0 \qquad\qquad\qquad as \;\; y \to \infty. \end{aligned} \tag{2.12}$$

A further transformation is needed for bodies with rounded lower ends because $\sin\phi/x$ approaches a constant value as x approaches zero [9]. The new non-dimensional variable is defined as [10].

$$F(x,y) = \frac{1}{x}\psi(x,y), \qquad G(x,y) = \frac{1}{x}N(x,y). \tag{2.13}$$

Substituting Equations (2.13) into Equations (2.8)-(2.11), one obtains

$$\begin{aligned} &[1+\Delta]\,\tfrac{\partial^3 F}{\partial y^3} + F\tfrac{\partial^2 F}{\partial y^2} - \left[\tfrac{\partial F}{\partial y}\right]^2 - K_1\tfrac{\partial F}{\partial y} + \Delta\tfrac{\partial G}{\partial y} \\ &+\tfrac{\theta_f \sin\phi}{x} = x\left[\tfrac{\partial F}{\partial y}\tfrac{\partial^2 F}{\partial x\partial y} - \tfrac{\partial F}{\partial x}\tfrac{\partial^2 F}{\partial y^2}\right], \end{aligned} \tag{2.14}$$

$$\lambda\frac{\partial^2 G}{\partial y^2} + F\frac{\partial G}{\partial y} - G\frac{\partial F}{\partial y} - \Delta.B\left[2G + \frac{\partial^2 F}{\partial y^2}\right] = x\left[\frac{\partial F}{\partial y}\frac{\partial G}{\partial x} - \frac{\partial G}{\partial y}\frac{\partial F}{\partial x}\right], \tag{2.15}$$

$$\frac{\partial^2\theta_f}{\partial y^2} + H\left[\theta_s - \theta_f\right] + \mathrm{Pr}\; F\frac{\partial\theta_f}{\partial y} = \mathrm{Pr}\, x\left[\frac{\partial F}{\partial y}\frac{\partial\theta_f}{\partial x} - \frac{\partial\theta_f}{\partial y}\frac{\partial F}{\partial x}\right], \tag{2.16}$$

$$\frac{\partial^2 \theta_s}{\partial y^2} - \chi H \left[\theta_s - \theta_f\right] = 0, \tag{2.17}$$

while the boundary conditions (2.12) become

$$\begin{array}{l} F = \frac{\partial F}{\partial y} = 0, \quad \theta_f = 1, \quad \theta_s = 1, \quad G + n\frac{\partial^2 F}{\partial y^2} = 0 \quad on \;\; y = 0, \\ \frac{\partial F}{\partial y} = 0, \quad \theta_f = 0, \quad \theta_s = 0, \quad G = 0 \qquad\qquad\qquad as \;\; y \to \infty. \end{array} \tag{2.18}$$

It should be noted here that $\lambda = 1 + \Delta/2$ as done by Cheng [11].

For cylinders of circular cross-section, $\sin\phi = \sin x$. However, for cylinders of elliptic cross-section, x and $\sin\phi$ can be given in terms of the eccentric angle α by the relations:

1. For blunt orientation

$$x = \int_0^{\alpha} (1 - e^2 \sin^2\gamma)^{1/2} d\gamma, \tag{2.19}$$

$$\sin\phi = \frac{b \sin\alpha}{a(1 - e^2 \sin^2\alpha)^{1/2}}. \tag{2.20}$$

2. For slender orientation

$$x = \int_0^{\alpha} (1 - e^2 \cos^2\gamma)^{1/2} d\gamma, \tag{2.21}$$

$$\sin\phi = \frac{\sin\alpha}{(1 - e^2 \cos^2\alpha)^{1/2}}. \tag{2.22}$$

Here, e denotes the eccentricity expressed as $e^2 = (1 - b^2/a^2)$, and b/a is the aspect ratio of the elliptic cylinder. When $x$approaches zero, as shown in Equations (2.19)-(2.22), the value of $\sin\phi/x$ approaches the aspect ratio b/a for the elliptic cylinder with blunt orientation while the value of $\sin\phi/x$ approaches the value of b^2/a^2 for the elliptic cylinder with slender orientation.

Of special significance in this type of problems are the local wall shear stress τ_w, the local wall couple stress M_w, the local rate of heat transfer for the fluid phase $(q_w)_f$, and the local rate of heat transfer for the solid phase $(q_w)_s$ which may be written respectively as

$$\tau_w = \left[(\mu + k)\frac{\partial \bar{u}}{\partial \bar{y}} + k\bar{N}\right]_{\bar{y}=0}, \tag{2.23}$$

$$M_w = -\gamma \left.\frac{\partial \bar{N}}{\partial \bar{y}}\right|_{\bar{y}=0}, \tag{2.24}$$

$$(q_w)_f = -k_f \left.\frac{\partial T_f}{\partial \bar{y}}\right|_{\bar{y}=0}, \tag{2.25}$$

$$(q_w)_s = -k_s \left.\frac{\partial T_s}{\partial \bar{y}}\right|_{\bar{y}=0}. \tag{2.26}$$

Using Equations (2.7) and (2.13), we have

$$\tau_w = \frac{\mu v}{a^2} Gr^{3/4} x \left[1 + \Delta(1-n)\right] \left.\frac{\partial^2 F}{\partial y^2}\right|_{y=0}, \tag{2.27}$$

$$M_w = -\frac{\gamma v}{a^3} Gr\, x \left.\frac{\partial G}{\partial y}\right|_{y=0}, \tag{2.28}$$

$$(q_w)_f = -\frac{k_f}{a} Gr^{1/4} \left[T_w - T_\infty\right] \left.\frac{\partial \theta_f}{\partial y}\right|_{y=0}, \tag{2.29}$$

$$(q_w)_s = -\frac{k_s}{a} Gr^{1/4} \left[T_w - T_\infty\right] \left.\frac{\partial \theta_s}{\partial y}\right|_{y=0}, \tag{2.30}$$

By means of Equations (2.27) and (2.28), we can define the local skin-friction coefficient Cf*and the local wall couple-stress coefficient Cg* as

$$C_f^* Gr^{3/4} = \frac{\tau_w}{\frac{\mu v}{a^2}} = x C_f = x\left[1 + \Delta(1-n)\right] \left.\frac{\partial^2 F}{\partial y^2}\right|_{y=0}, \tag{2.31}$$

$$C_g^* Gr = -\frac{M_w}{\frac{\gamma v}{a^3}} = x C_g = -x \left.\frac{\partial G}{\partial y}\right|_{y=0} \tag{2.32}$$

In addition, the local Nusselt number for the fluid can be written as

$$Nu_f = \frac{a(q_w)_f}{k_f \left[T_w - T_\infty\right]}. \tag{2.33}$$

Using Equation (2.29), we obtain

$$\frac{Nu_f}{Gr^{1/4}} = -\left.\frac{\partial \theta_f}{\partial y}\right|_{y=0}. \tag{2.34}$$

Similarly, the local Nusselt number for the solid matrix can be written as

$$Nu_s = \frac{a(q_w)_s}{k_s \left[T_w - T_\infty\right]}. \tag{2.35}$$

and by using Equation (2.30), we obtain

$$\frac{Nu_s}{Gr^{1/4}} = -\left.\frac{\partial \theta_s}{\partial y}\right|_{y=0}. \tag{2.36}$$

Table 1
Comparison of the local Nusselt number for the Newtonian fluid case with H=0, K1=0, Pr=1.0.

α	$b/a = 0.1$ (blunt)	$b/a = 0.25$ (blunt)	$b/a = 0.5$ (blunt)	$b/a = 1.0$ (slender)
0.0	0.2373	0.2979	0.3543	0.4213
	[0.2375]	[0.2979]	[0.3542]	[0.4213]
	(0.2369)	(0.2979)	(0.3542)	(0.4212)
0.4	0.2419	0.3037	0.3592	0.4282
	[0.2418]	[0.3034]	[0.3589]	[0.4183]
	(0.2421)	(0.3039)	(0.3593)	(0.4182)
0.8	0.2561	0.3240	0.3747	0.4093
	[0.2607]	[0.3240]	[0.3747]	[0.4093]
	(0.2599)	(0.3240)	(0.3747)	(0.4093)
1.2	0.3036	0.3675	0.3979	0.3941
	[0.3044]	[0.3677]	[0.3985]	[0.3942]
	(0.3031)	(0.3673)	(0.3984)	(0.3942)
2.0	0.3212	0.3659	0.3693	0.3441
	[0.3220]	[0.3670]	[0.3712]	[0.3440]
	(0.3206)	(0.3670)	(0.3713)	(0.3443)
2.4	0.2362	0.2838	0.3073	0.3073
	[0.2360]	[0.2836]	[0.3078]	[0.3066]
	(0.2361)	(0.2840)	(0.3081)	(0.3073)
π	0.1206	0.1501	0.1745	0.1963
	[0.1201]	[0.1500]	[0.1744]	[0. 1963]
	(0.1206)	(0.1504)	(0.1746)	(0.1963)

Results in brackets are those of Bhattacharyya and Pop [9] and results in parentheses are those of Merkin [10]

The solution of the problem is obtained by solving the system of equations (14)-(17) along with the boundary conditions (18) numerically by means of an efficient, iterative, tri-diagonal implicit finite difference method discussed previously by Blottner [12]. In order to check the accuracy of the numerical method, the local Nusselt number of the fluid phase for a Newtonian fluid (is compared with those reported earlier by Bhattacharyya and Pop [9] and Merkin [10] using the thermal-equilibrium model. As shown in Table 1, the present results are found to be in excellent agreement with the results of Bhattacharyya and Pop [9] and Merkin [10].

3 Results and Discussion

Numerical computations are carried out and a parametric study is performed to illustrate the influence of the physical parameters on the linear and angular velocities and the fluid- and solid-phase temperatures, as well as the local skin-friction coefficient, wall couple-stress coefficient, and the local Nusselt numbers for fluid and solid phases. The results of this parametric study are shown in Figs. 2-25.

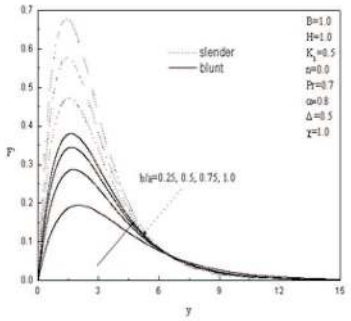

Fig. 2. Linear velocity profiles for different values of aspect ratio

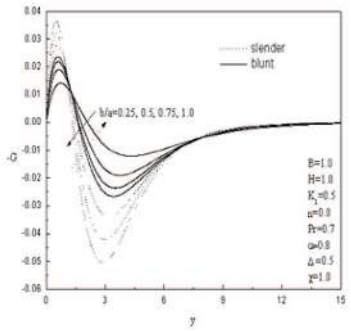

Fig. 3. Angular velocity profiles for different values of aspect ratio

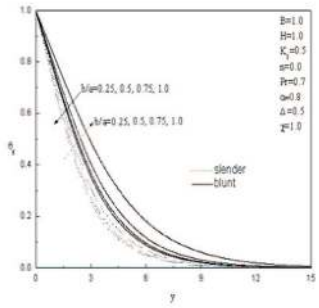

Fig. 4. Fluid-phase temperature profiles for different values of aspect ratio

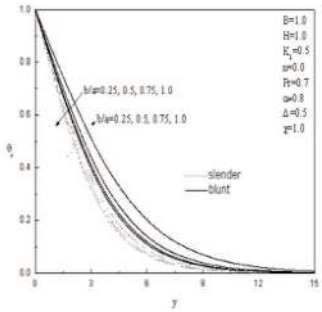

Fig. 5. Solid-phase temperature profiles for different values of aspect ratio

Figures 2-5 present typical profiles for the linear velocity, angular velocity, fluid-phase temperature, and solid-phase temperature for different values of the aspect ratio $b/a$and blunt and slender cylinder orientations, respectively. It is clearly observed that different behaviors take place depending on the cylinder orientation. For a blunt cylinder orientation, the linear velocity (F') increases whereas the angular velocity (G), fluid-phase temperature (θ_f), and the solid-phase temperature (θ_s) decrease as the cylinder aspect ratio b/aincreases. On the other hand, the exact opposite effect is obtained for a slender cylinder orientation for which the profiles of G, θ_f and θ_s increase while the profile of F' decreases as the cylinder aspect ratio b/a increases.

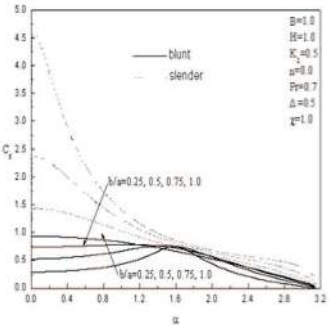

Fig. 6. Local skin-friction coefficient distribution for various aspect ratios

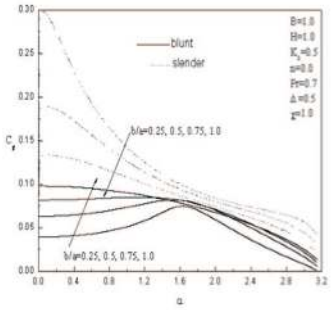

Fig. 7. Local couple-stress coefficient distribution for various aspect ratios

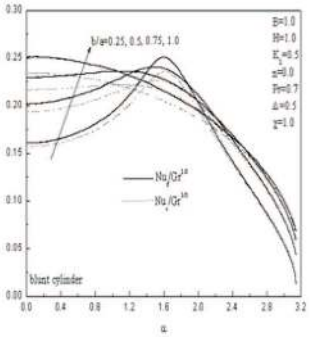

Fig. 8. Local fluid- and solid-phase Nusselt numbers distributions for blunt cylinders and various aspect ratios

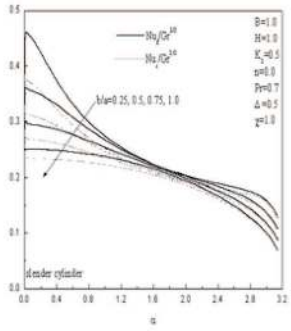

Fig. 9. Local fluid- and solid-phase Nusselt numbers distributions for slender cylinders and various aspect ratios

Figures 6-9 illustrate the effects of the cylinder aspect ratio b/a on the distributions of the local skin-friction coefficientC_f, local couple-stress coefficientC_g, and local Nusselt numbers for the fluid and solid phases $Nu_f/Gr^{1/2}$and $Nu_s/Gr^{1/2}$along the cylinder for blunt and slender cylinder orientations, respectively. The trends of C_f,C_g, $Nu_f/Gr^{1/2}$and $Nu_s/Gr^{1/2}$along the cylinder depend strongly on the cylinder orientation. In general, for a blunt cylinder orientation and$0 \leq b/a \leq 1$, the values of C_f, C_g, $Nu_f/Gr^{1/2}$and $Nu_s/Gr^{1/2}$tend to increase as the eccentric angle α increases reaching a maximum at around $\alpha = \pi/2$ and then decrease thereafter reaching a minimum at $\alpha = \pi$. However, for a slender cylinder orientation, the values of C_f,C_g, $Nu_f/Gr^{1/2}$and $Nu_s/Gr^{1/2}$are maxima at small values of the eccentric angle α and they decrease as α increases further reaching their minima at $\alpha = \pi$. As the cylinder aspect ratio b/a increases, the values of C_f, C_g, $Nu_f/Gr^{1/2}$and $Nu_s/Gr^{1/2}$increase for a blunt cylinder orientation while they decrease for a slender cylinder orientation. The local Nusselt number values for the solid phase

are lower than those for the fluid phase. Also, the values of C_f, C_g, $Nu_f/Gr^{1/2}$and $Nu_s/Gr^{1/2}$for a slender cylinder orientation are higher than those corresponding to a blunt cylinder orientation. All these behaviors are clearly shown in Figs. 6-9.

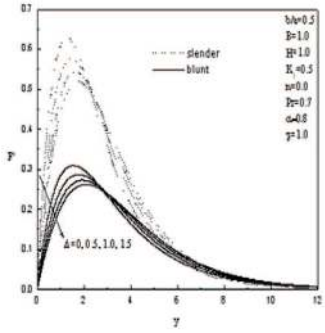

Fig. 10. Effects of vortex-viscosity parameter on linear velocity profiles

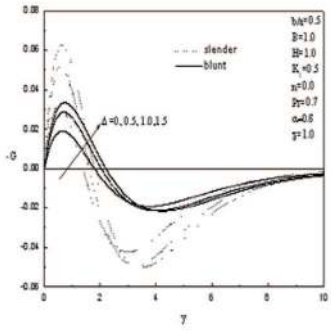

Fig. 11. Effects of vortex-viscosity parameter on angular velocity profiles

Figures 10 and 11 present the effects of the micropolar fluid vortex-viscosity parameterΔ on the linear and angular velocity profiles for both blunt and slender cylinder orientations, respectively. It should be noted that Δ=0 corresponds to the case of a Newtonian fluid. Physically, increasing the values of Δ has the tendency to increase the viscous effects in the boundary layer close to the cylinder surface which in turn, causes decreases in the linear and angular velocities (F' and G). However, far downstream, this effect decreases and an increasing trend in the linear and angular velocities is predicted. These behaviors are true regardless of the cylinder orientation as is clear from Figs. 10 and 11.

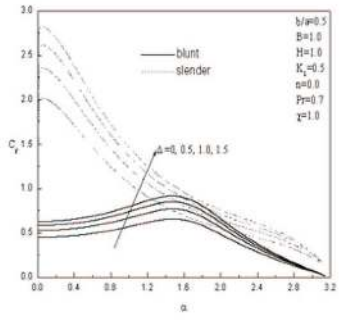

Fig. 12. Effects of vortex-viscosity parameter on local skin-friction coefficient

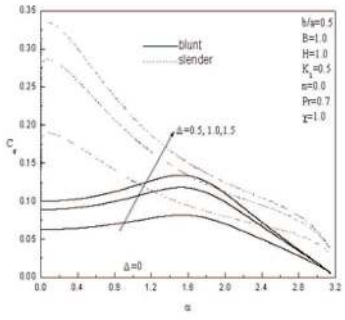

Fig. 13. Effects of vortex-viscosity parameter on local couple-stress coefficient

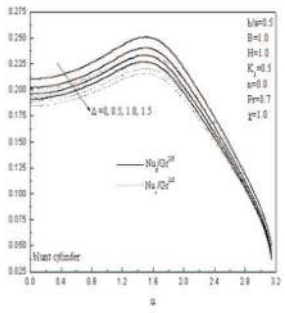

Fig. 14. Effects of vortex-viscosity parameter on local fluid- and solid-phase Nusselt numbers for blunt cylinders

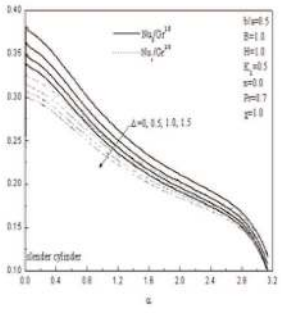

Fig. 15. Effects of vortex-viscosity parameter on local fluid- and solid-phase Nusselt numbers for slender cylinders

Figures 12-15 depict the influence of the micropolar fluid vortex-viscosity parameter Δ on the distributions of the local skin-friction coefficient C_f, local couple-stress coefficient C_g, and local Nusselt numbers for the fluid and solid phases $Nu_f/Gr^{1/2}$and $Nu_s/Gr^{1/2}$along the cylinder for blunt and slender cylinder orientations, respectively. It is predicted that the local skin-friction and couple-stress coefficients increase whereas the local Nusselt numbers for the fluid and solid phases decrease as the vortex-viscosity parameterΔ increases. This prediction is true for both blunt and slender cylinder orientations.

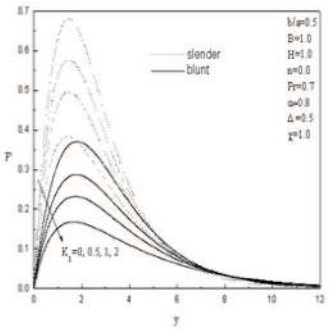

Fig. 16. Effects of permeability parameter on linear velocity profiles

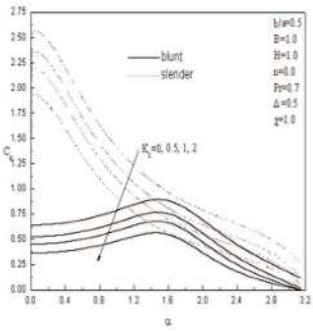

Fig. 17. Effects of permeability parameter on local skin-friction coefficient

Figure 16 displays the effects of the permeability parameter K_1on the linear velocity profiles for both blunt and slender cylinder orientations. The presence of the porous medium represents an obstacle to flow and, as a result, reduces its velocity. This is depicted in the decreases in the linear velocity profiles asK_1increases, as shown in Fig. 16.

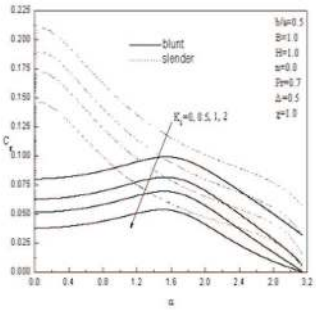

Fig. 18. Effects of permeability parameter on local couple-stress coefficient

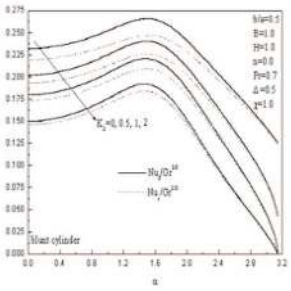

Fig. 19. Effects of permeability parameter on local fluid- and solid-phase Nusselt numbers for blunt cylinders

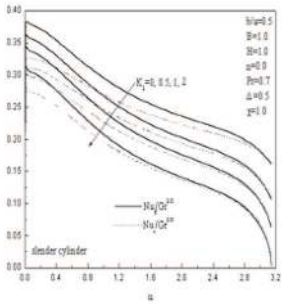

Fig. 20. Effects of permeability parameter on local fluid- and solid-phase Nusselt numbers for slender cylinders

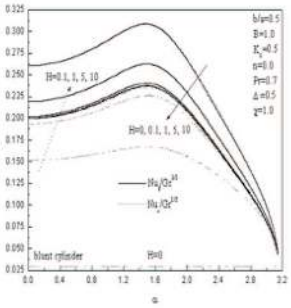

Fig. 21. Effects of heat transfer coefficient on local fluid- and solid-phase Nusselt numbers for blunt cylinders

The effects of the presence of the porous medium represented by the permeability parameter K_1 on the distributions of the local skin-friction coefficient C_f, local couple-stress coefficient C_g, and local Nusselt numbers for the fluid and solid phases $Nu_f/Gr^{1/2}$and $Nu_s/Gr^{1/2}$along the cylinder for blunt and slender cylinder orientations are elucidated in Figs. 17-20, respectively. It is observed that the values ofC_f,C_g, $Nu_f/Gr^{1/2}$and $Nu_s/Gr^{1/2}$tend to decrease as K1 increases and that is true for both blunt and slender cylinder orientations.

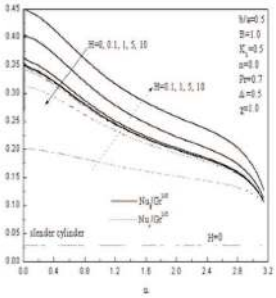

Fig. 22. Effects of heat transfer coefficient on local fluid- and solid-phase Nusselt numbers for slender cylinders

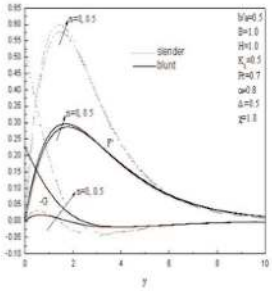

Fig. 23. Effects of micro-gyration boundary parameter on linear and angular velocity profiles

Figures 21 and 22 depict the effects of the heat transfer coefficient between the fluid and solid phases Hon the local Nusselt number distributions of both the fluid and solid phases along the cylinder for blunt and slender cylinder orientations, respectively. Obviously, an energy balance for the fluid and solid phases indicates that heat loss from the fluid phase is gained by the solid phase. The case $H = 0$represents the case of thermal equilibrium. As Hincreases, the fluid-phase Nusselt number decreases while the solid-phase Nusselt number increases by virtue of inter-phase heat transfer. As$H \to \infty$, then the temperatures of both phases become the same. This gives equal Nusselt numbers of both phases. This behavior is true for both blunt and slender cylinder orientations as is obvious from Figs. 21 and 22.

The effects of the micro-gyration boundary parameter n on the linear and angular velocity profiles for both blunt and slender cylinder orientations are displayed in Fig. 23. As expected, the wall value of the angular velocity is strongly affected by changes in the value of n. A comparison of the values of the linear velocity for strong concentration of microelement ($n = 0$) and weak concentration of microelement ($n = 0.5$) shows that the values of the linear velocity for $n = 0.5$ are larger than those corresponding to $n = 0$. However, the angular velocity (G) decreases as n increases. In addition, for a slender cylinder orientation, the angular velocity profiles are completely negative in the case of weak concentration of microelement ($n = 0.5$), while it is positive and negative in the case of strong concentration of microelement ($n = 0$).

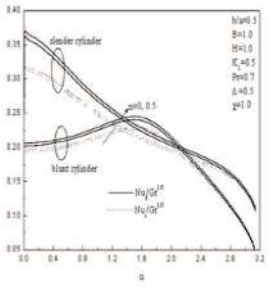

Fig. 24. Effects of micro-gyration boundary parameter on local fluid- and solid-phase Nusselt numbers

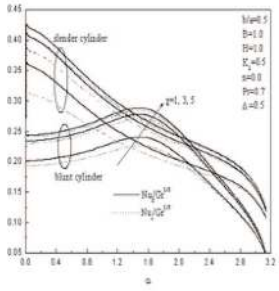

Fig. 25. Effects of thermal conductivity ratio on local fluid- and solid-phase Nusselt numbers

Figures 24 and 25 show the effects of the micro-gyration boundary parameter n and the thermal conductivity ratio χ on the local Nusselt number for the fluid phase $Nu_f/Gr^{1/4}$and the local Nusselt number for the solid phase $Nu_s/Gr^{1/4}$for blunt and slender cylinder orientations, respectively. From these figures, it is observed that increasing either the thermal conductivity ratio χ or the micro-gyration boundary parameter n results in increases in the local Nusselt numbers of the fluid and solid phases for both blunt and slender cylinder orientations.

4 Conclusions

Heat transfer by free convection boundary-layer flow of a micropolar fluid along a cylinder of elliptic cross-section embedded in porous media was studied using the thermal non-equilibrium model. An appropriate coordinate transformation was employed to transform the governing equations into non-dimensional non-similar boundary-layer equations. The obtained boundary-layer equations were then solved numerically by an efficient implicit finite-difference method. From the results of the problem the following conclusions were observed:

1. The linear velocity increased due to increases in the cylinder aspect ratio and the micro-gyration boundary parameter and decreased as either the permeability parameter or the vortex-viscosity parameter was increased.
2. The angular velocity profiles were completely negative for the case of weak concentration of microelement, while it was positive and negative in the case of strong concentration of microelement.
3. The local skin-friction coefficient and the local wall couple-stress coefficient increased as either the cylinder aspect ratio or the vortex-viscosity parameter decreased due to increases in either of the permeability parameters.
4. The local fluid-phase Nusselt number increased as either the micro-gyration boundary parameter, thermal conductivity ratio or the cylinder aspect ratio (for blunt orientation and small eccentric angles) increased, and decreased as either the vortex-viscosity parameter, permeability parameter, heat transfer coefficient or the cylinder aspect ratio for slender cylinder orientation increased.

5. The local solid-phase Nusselt number increased as either the micro-gyration boundary parameter, thermal conductivity ratio or the heat transfer coefficient increased, and decreased as either the vortex-viscosity parameter, cylinder aspect ratio (for slender orientation), or the permeability parameter increased.

6. The local skin-friction coefficient, local wall couple-stress coefficient and the local Nusselt numbers of the fluid and solid phases of elliptic cylinders with a slender orientation were found to be higher than those with a blunt orientation.

References

[1] A. C. Eringen, "Simple Microfluids", Int. J. Eng. Sci. 2, 205-217, (1964).

[2] A. C. Eringen,"Theory of micropolar fluids", J. Math. Mech. 16, 1-18, (1966).

[3] M. Quintard and S. Whitaker, "One- and two-equation models for transient diffusion processes in two-phase system", Adv. Heat Transfer 23, 369-464, (1993).

[4] A. Amiri and K. Vafai, "Transient analysis of incompressible flow through a packed bed", Int. J. Heat Mass Transfer 41, 4259-4279, (1998).

[5] S. J. Kim and D. Y. Lee, "On the local thermal equilibrium microchannel heats sinks", Int. J. Heat Mass Transfer 43, 1735-1748, (2000).

[6] E. U. Schlunder, "Equivalence of one- and two-phase models for heat transfer processes in packed beds: one-dimensional theory", Chem. Eng. Sci. 30, 449-452, (1975).

[7] M. Quintard, "Modelling local non-equilibrium heat transfer in porous media", Proceeding of the 11th International Heat Transfer Conference 1, 279-285, (1998).

[8] D. Y. Lee and K. Vafai, "Analytical characterization and conceptual assessment of solid and fluid temperature differentials in porous media", Int. J. Heat Mass Transfer 42, 423-435, (1999).

[9] S. Bhattacharyya and I. Pop, "Free convection from cylinders of elliptic cross-section in micropolar fluids", Int. J. Eng Sci. 34, 1301-1310, (1996).

[10] J. H. Merkin, "Free convection boundary layers on cylinders of elliptic cross-section", ASME J. Heat Transfer 99, 453-457, (1977).

[11] C.-Y. Cheng, "Natural convection heat and mass transfer from a sphere in micropolar fluids with constant wall temperature and concentration", Int. Commun. Heat Mass Transfer 35, 750-755, (2008).

[12] F. G. Blottner, "Finite-difference methods of solution of the boundary-layer equations" AIAA Journal 8, 193-205, (1970).